$A_2CuP_3S_9$ (A = K, Rb), $Cs_2Cu_2P_2S_6$, and $K_3CuP_2S_7$: New Phases from the Dissolution of Copper in Molten Polythiophosphate Fluxes

Jason A. Hanko,[†] Julien Sayettat,[‡] Stéphane Jobic,[‡] Raymond Brec,[‡] and Mercouri G. Kanatzidis*,[†]

Department of Chemistry and Center for Fundamental Materials Research, Michigan State University, East Lansing, Michigan, 48824, and Institut des Matériaux de Nantes, BP 32229 44322 Nantes Cedex 03, France

Received March 23, 1998. Revised Manuscript Received June 15, 1998

The reaction of Cu with a molten mixture of A_2S/P_2S_5 (A = K, Rb, Cs) produced the quaternary compounds $A_2CuP_3S_9$ (A = K, Rb) and $Cs_2Cu_2P_2S_6$. The reaction of Cu with a molten mixture of $K_2S/P_2S_5/S$ produced the quaternary compound $K_3CuP_2S_7$. $A_2CuP_3S_9$ (A = K, Rb); **I**, **II**, respectively) crystallizes in the space group $P2_1/n$ (no. 14) for **I**: a = 6.8331(6) Å, b = 23.562(2) Å, c = 9.5415(7) Å, β = 100.242(7)°, Z = 4, V = 1511.8(4) Å^3, ρ_{calc} = 2.298 g/cm^3. $Cs_2Cu_2P_2S_6$ (**III**) crystallizes in the space group $P2_1/c$ (no. 14) with a = 9.538(3) Å, b = 12.793(4) Å, c = 10.429(4) Å, β = 103.76(2)°, Z = 4, V = 1236.1(7) Å^3, ρ_{calc} = 3.478 g/cm^3. $K_3CuP_2S_7$ (**IV**) crystallizes in the space group $P2_1/a$ (no. 14) with a = 13.113(5) Å, b = 6.702(3) Å, c = 15.141(7) Å, β = 115.13(1)°, Z = 4, V = 1315(1) Å^3, ρ_{calc} = 2.35 g/cm^3. The structure of **I**−**II** consists of novel one-dimensional $[CuP_3S_9]_n^{2n-}$ chains separated by A^+ cations. The chains run along the crystallographic b-axis. The Cu^+ cation is in tetrahedral coordination with the cyclic $[P_3S_9]^{3-}$ anion, a new polythiophosphate unit. The structure of **III** has one-dimensional $[Cu_2P_2S_6]_n^{2n-}$ chains separated by Cs^+ cations. The chains consists of alternating $[Cu_2]^{2+}$ dimers linked by the ethane-like $[P_2S_6]^{4-}$ units. The structure of **IV** is also one-dimensional, with $[CuP_2S_7]_n^{3n-}$ chains separated by K^+ ions. The Cu^+ ions are in a slightly distorted trigonal planar environment with the $[P_2S_7]^{4-}$ units. Differential thermal analysis, far-IR, Raman spectroscopy, and optical spectroscopic data are reported. The results of a band structure calculation at the DFT-LMTO level for $K_2CuP_3S_9$ are also discussed.

1. Introduction

The recent application of chalcophosphate fluxes to solid-state synthesis has uncovered a multitude of new materials with elaborate structure types arising from a large variety of new binding modes displayed by the $[P_xQ_y]_n^{n-}$ (Q = S, Se) units.[1] An interesting trend, which has become evident from this work, is that the $[P_xSe_y]_n^{n-}$ species behave very differently from the corresponding $[P_xS_y]_n^{n-}$ species. This trend is manifested not only in how the $[P_xQ_y]_n^{n-}$ (Q = S, Se) anions bind to metal ions but also with respect to their relative stability. For example, the tetrahedral units $[PS_4]^{3-}$ and $[PSe_4]^{3-}$ often do not lead to the same structure types when they form compounds of the same formula. In fact, they do not even tend to give compounds with the same formula. This phenomenon is reminiscent of the similar differences previously observed between the polychalcogenide S_n^{2-} and Se_n^{2-} species.[2] Furthermore, the analogous synthetic conditions that give rise to a certain $[P_xSe_y]^{z-}$ unit tend to give rise to a different $[P_xS_y]^{z-}$ unit. Often the sulfide and selenide anions differ in the oxidation state of the phosphorus atom.[3] The latter is the consequence of the difference in the electronegativity between the S and Se atoms. These facts underscore the need for the exploration of both the thiophosphate and selenophosphate fluxes for the same metal system, and the continued search for fundamental differences in chemistry and reactivity.

In general, the polychalcophosphate fluxes are formed by the in situ fusion of $A_2Q/P_2Q_5/Q$ (A = K, Rb, Cs; Q = S, Se) and contain various $[P_xQ_y]^{n-}$ units available for reaction with metal ions. Typically, this type of coordination chemistry leads to anionic frameworks stabilized by alkali metal cations. The generality of this method has been demonstrated by the ability to incor-

* To whom correspondence should be addressed.
[†] Department of Chemistry.
[‡] Institut des Matériaux de Nantes.

(1) (a) Kanatzidis, M. G. *Curr. Opinion Solid State and Mater. Sci.* **1997**, *2*, 139; (b) Sutorik, A. C.; Kanatzidis, M. G. *Prog. Inorg. Chem.* **1995**, *43*, 151−265.

(2) Kanatzidis, M. G.; Huang, S.-P. *Coord. Chem. Rev.* **1994**, *130*, 509.

(3) Chondroudis, K.; Hanko, J. A.; Kanatzidis, M. G. *Inorg. Chem.* **1997**, *36*, 2623−2632.

(4) (a) McCarthy, T. J.; Kanatzidis, M. G. *Chem. Mater.* **1993**, *5*, 1061−1063; (b) McCarthy, T. J.; Kanatzidis, M. G. *J. Chem. Soc. Chem. Commun.* **1994**, 1089−1090; (c) McCarthy, T. J.; Hogan, T.; Kannewurf, C. R.; Kanatzidis, M. G. *Chem. Mater.* **1994**, *6*, 1072−1079; (d) McCarthy, T. J.; Kanatzidis, M. G. *J. Alloys Comp.* **1996**, 236, 70−85; (e) Chondroudis, K.; McCarthy, T. J.; Kanatzidis, M. G. *Inorg. Chem.* **1996**, *35*, 840−844; (f) Chondroudis, K.; Kanatzidis, M. G. *J. Chem. Soc. Chem. Commun.* **1996**, 1371−1372.

10.1021/cm980175w CCC: $15.00
Published on Web 08/29/1998

porate main group,[4] transition,[5] lanthanide, and actinide[6] metals into solid-state chalcophosphate compounds. The highly basic nature of the fluxes permits the suppression of the highly stable $M_2P_2Q_6$ (Q = S, Se) phases. The $M_2P_2Q_6$ (Q = S, Se) structure type is related to that of CdI_2,[7,8] with alternating, octahedrally coordinated, metal ions and the ethane-like $[P_2Q_6]^{4-}$ (Q = S, Se) units. Some compounds possess interesting magnetic properties[9] and intercalation chemistry,[10] whereas others have been studied intensively as potential candidates for cathode materials in secondary lithium batteries.[11] Substitution on the divalent metal cations by monovalent coinage metal cations results in $M'_4P_2Q_6$ (e.g., M′ = Ag, Q = S; M′ = Cu, Q = Se).[12] Their structure retains the basic $M_2P_2Q_6$ motif, but now each octahedral metal site is replaced by two M'^{+} ions with trigonal planar coordination. The two divalent metal ions can also be replaced by a monovalent coinage and a trivalent main group metal ion to give $M'M''P_2Q_6$, again retaining the overall $M_2P_2Q_6$ structure type.[13] In a departure from the norm, Cu forms two isostructural compounds with $[PQ_4]^{3-}$ units in Cu_3PQ_4.[14]

Because of the great utility of the alkali thiophosphate flux approach for the exploration of multinary phases we applied it to the copper chalcophosphate systems. The reaction of the coinage metals with polychalcophosphate fluxes has already resulted in a number of unusual compounds; examples include $Cs_2M_2P_2Se_6$ (M = Cu, Ag),[5a] $A_3AuP_2Se_8$ (A = K, Rb, Cs),[3] $A_2Au_2P_2Se_6$ (A = Rb, Cs),[3] $K_3Ag_3P_3Se_9$,[5a] $K_3Cu_3P_3Se_9$,[5e] $K_2Cu_2P_4Se_{10}$,[5f] A_2AuPS_4 (A = K, Rb, Cs),[3] $AAuP_2S_7$ (A = K, Rb),[3] and, recently, $KAu_5P_2S_8$.[15] An interesting counterion effect exists in the $A_3M_3P_3S_9$ system. The large Cs^+ counterion gives $[M_2P_2Se_6]_n^{2n-}$ (M = Cu, Ag) consisting of infinite chains of alternating $[P_2Se_6]^{4-}$ units and M_2^{2+} dimers. Upon moving to the smaller K^+ cation, the $K_3M_3P_3Se_9$ (M = Cu,[5e] Ag[5a]) adopts a three-dimensional structure comprised of ethane-like $[P_2Se_6]^{4-}$ units and tetrahedral Cu^+ or Ag^+ ions in a complex but elegant bonding scheme. Although one might expect that the thiophosphate and selenophosphate systems would produce isostructural compounds, the gold chalcophosphates[3] provide an excellent example of how chemically divergent the chemistry of the two systems can be. The chemistry of copper presents similar differences between the sulfur and selenium systems. Here, we report the synthesis, structures, spectroscopic and thermal properties of the new quaternary compounds $A_3CuP_3S_9$ (A = K, Rb), $Cs_2Cu_2P_2S_6$, and $K_3CuP_2S_7$. Although the selenide analogue of $Cs_2Cu_2P_2S_6$ has already been reported, the selenide analogues for $A_3CuP_3S_9$ (A = K, Rb) and $K_3CuP_2S_7$ are unknown and it seems unlikely that they would be stable. The $K_2CuP_3S_9$ features the rare cyclic $[P_3S_9]^{3-}$ anion. The results of the band structure calculation for this compound are also discussed.

2. Experimental Section

2.1. Reagents. The reagents mentioned in this study were used as obtained unless noted otherwise.

2.2. Syntheses. A_2S (A = K, Rb, Cs) were prepared by reacting stoichiometric amounts of the elements in liquid ammonia as described elsewhere.[3]

Preparation of $K_2CuP_3S_9$ (I). An amount of 0.032 g (0.50 mmol) of Cu, 0.333 g (1.50 mmol) of P_2S_5, and 0.110 g (1 mmol) of K_2S were thoroughly mixed and sealed under vacuum in a Pyrex tube. The reaction mixture was heated to 550 °C for 4 days, followed by cooling to 150 °C at a rate of 4 °C/h. The excess $K_x[P_yS_z]$ flux was removed by washing with deaerated methanol under an inert atmosphere revealing yellow crystals (75% yield based on Cu). The yellow crystals are stable in air for several months but decompose in the presence of water. The product is occasionally contaminated with brown-orange crystals of Cu_3PS_4 and/or a black powder.

Preparation of $Rb_2CuP_3S_9$ (II). An amount of 0.032 g (0.50 mmol) of Cu, 0.220 g (1 mmol) of P_2S_5, and 0.203 g (1 mmol) of Rb_2S was sealed under vacuum in a Pyrex tube and heated as for **I**. The product, which is stable in air but decomposes in the presence of water, was isolated as for **I** above to give yellow crystals (52% yield based on Cu).

Preparation of $Cs_2Cu_2P_2S_6$ (III). A mixture of 0.032 g (0.50 mmol) of Cu, 0.330 g (1.50 mmol) of P_2S_5, and 0.298 g (1 mmol) of Cs_2S were sealed under vacuum in a Pyrex tube and heated as for **I**. The product was isolated as for **I** to give a mixture of dark violet and yellow crystals. The mixture was immediately washed with deaerated water to give dark violet crystals in ~50% yield based on Cu. The resulting dark violet crystals are stable in air and water.

Preparation of $K_3CuP_2S_7$ (IV). $K_3CuP_2S_7$ was synthesized from a mixture of 0.016 g (0.25 mmol) of Cu, 0.110 g (0.50 mmol) of P_2S_5, 0.550 g (0.50 mmol) of K_2S, and 0.048 g (1.5 mmol) of S that was sealed under vacuum in a Pyrex tube. The reaction was heated to 500 °C for 4 days, followed by cooling to 110 °C at a rate of 4 °C/h. The product is stable in air but decomposes in water. The compound was isolated as for **I** above to give transparent colorless crystals (40% yield based on Cu).

2.3 Physical Measurements and Calculations. The compounds were examined by powder X-ray diffraction to

(5) (a) McCarthy, T. J.; Kanatzidis, M. G. *Inorg. Chem.* **1995**, *34*, 1257−1267; (b) Chondroudis, K.; Kanatzidis, M. G. *Inorg. Chem.* **1995**, *34*, 5401−5402; (c) Chondroudis, K.; McCarthy, T. J.; Kanatzidis, M. G. *Inorg. Chem.* **1995**, *35*, 3451; (d) Chondroudis, K.; Kanatzidis, M. G. *Angew. Chem.* **1997**, *36*, 1324; (e) Dorhout, P. K.; Malo, T. M. *Z. Anorg. Allg. Chem.* **1996**, *622*, 385; (f) Chondroudis, K.; Kanatzidis, M. G. *Inorg. Chem.* **1998**, *37*, 2098.

(6) (a) Chondroudis, K.; Kanatzidis, M. G. *C. R. Acad. Sci. Paris, Series B* **1996**, *322*, 887−894; (b) Chondroudis, K.; Kanatzidis, M. G. *J. Chem. Soc. Chem.* **1997**, *119*, 2574−2575; (c) Chen, J. H.; Dorhout, P. K. *Inorg. Chem.* **1995**, *34*, 5705; (d) Chen, J. H.; Dorhout, P. K.; Ostenson, J. E. *Inorg. Chem.* **1996**, *35*, 5627.

(7) (a) Klingen, W.; Eulenberger, G.; Hahn, H. *Z. Anorg. Allg. Chem.* **1973**, *401*, 97−112; (b) Toffoli, P.; Khodadad, P.; Rodier, N. *Acta Crystallogr., Sect. B*, **1978**, *34*, 1779−1781; (c) Klimgen, W.; Ott, R.; Hahn, H. *Z. Anorg. Allg. Chem.* **1973**, *396*, 271−278; (d) Jandali, M. Z.; Eulenberger, G.; Hahn, H. *Z. Anorg. Allg. Chem.* **1978**, *447*, 105−118.

(8) (a) Ouvrard, G.; Brec, R.; Rouxel, J. *Mater. Res. Bull.* **1985**, *20*, 1181−1189; (b) Lee, S.; Colombet, P.; Ouvrard, G.; Brec, R. *Inorg. Chem.* **1988**, *27*, 1291−1294; (c) Lee, S.; Colombet, P.; Ouvrard, G.; Brec, R. *Mater. Res. Bull.* **1986**, *21*, 917−928; (d) Durand, E.; Ouvrard, G.; Evain, M.; Brec, R. *Inorg. Chem.* **1990**, *29*, 4916−4920.

(9) (a) Odile, J.-P.; Steger, J. J.; Wold, A. *Inorg. Chem.* **1975**, *14*, 2400−2402; (b) Taylor, B. E.; Steger, J. J.; Wold, A.; Kostiner, E. *Inorg. Chem.* **1974**, *13*, 2719−2721; (c) Taylor, B. E.; Steger, J. J.; Wold, A. *J. Solid State Chem.* **1973**, *7*, 461−467.

(10) (a) Lagadic, I.; Leaustic, A.; Clement, R. *J. Chem. Soc., Chem. Commun.* **1992**, 1396−1397; (b) Clement, R.; Audiere, J.-P.; Renard, J.-P. *Rev. Chim. Miner.* **1982**, *19*, 560−571; (c) Michalowicz, A.; Clement, R. *Inorg. Chem.* **1982**, *21*, 3872−3877; (d) Clement, R. *J. Chem. Soc., Chem. Commun.* **1980**, 647−648; (e) Joy, P. A.; Vasudevan, S.. *J. Chem. Soc. Chem.* **1981**, *104*, 7792−7801.

(11) Thompson, A. H.; Whittingham, M. S. U.S. Patent 4,049,879, **1977**; (b) Brec, R.; Le Mehaute′. A. Fr. Patent 7,704,519, 1977.

(12) Toffoli, P.; Michelet, A.; Khodadad, P.; Rodier, N. *Acta Crystallogr.* **1982**, *B38*, 706−710.

(13) (a) Pfeiff, R.; Kniep, R.. *J. Alloys Comp.* **1992**, 186, 111−133; (b) Evain, M.; Boucher, F.; Brec, R.; Mathey, Y. *J. Solid State Chem.* **1991**, *90*, 8−16; (c) Lee, S.; Colombet, P.; Ouvrard, G.; Brec, R. *Mater. Res. Bull.* **1986**, *21*, 917−928; (d) Leblanc, A.; Ouili, Z.; Colombet, P. *Mater. Res. Bull.* **1985**, *20*, 947−954.

(14) (a) Ferrari, A.; Cavalca L. *Gazzetta Chemica Italiana* **1948**, *78*, 283−285; (b) Garin, J.; Parthe, E. *Acta Crystallogr.* **1972**, *B28*, 3672−3674.

(15) Lõken, S.; Tremel W., *Eur. J. Inorg. Chem.* **1998**, 283−289.

Table 1. Crystallographic Data for I, III, and IV

formula	$K_2CuP_3S_9$ (**I**)	$Cs_2Cu_2P_2S_6$ (**III**)	$K_3CuP_2S_7$ (**IV**)
FW	523.20	647.21	467.21
a, Å	6.8331 (6)	9.538 (3)	13.113 (6)
b, Å	23.562 (2)	12.793 (4) Å	6.702 (9)
c, Å	9.5415 (7)	10.429 (2) Å	15.141 (8)
α (deg)	90.00	90.00	90.00
β (deg)	100.242 (7)	103.76 (2)°	98.71 (4)
γ (deg)	90.00	90.00	90.00
Z, V(Å^3)	4; 1151.8(7)	4; 1236.1 (7)	4; 1315 (2)
(*λ*), Å	0.71069	0.71069	0.71069
space group	$P2_1/n$ (no. 14)	$P2_1/c$ (no. 14)	$P2_1/a$ (no. 14)
D_{calc}, g/cm^3	2.298	3.478	2.359
μ, cm^{-1}	35.2	10.46	39.16
$2\Theta_{max}$, deg	56.3	40	50
temp, °C	23	23	23
final R/R_w, %[a]	3.4/3.6	2.3/2.8	4.1/3.7

[a] $R = \Sigma(|F_o| - |F_c|)/\Sigma|F_o|$, $R_w = \{\Sigma w(|F_o| - |F_c|)^2/\Sigma w|F_o|^2\}^{1/2}$.

check for phase purity. Accurate *d* spacings obtained from the powder pattern for **I** were recorded on a CPS 120 INEL X-ray powder diffractometer using monochromatized radiation Cu $K\alpha_1$ ($\lambda = 1.540598$ Å). Accurate *d* spacings obtained from the powder patterns for **III**−**IV** were recorded on a Phillips XRG-3000 computer-controlled powder diffractometer with Ni filtered Cu Kα radiation. Both diffractometers are equipped with a curved position-sensitive detector calibrated with $Na_2Ca_3Al_{12}F_{14}$. The calculated powder patterns were calculated either with the Lazy Pulverix Program[16a] or with the CERIUS[2] software.[16b] Tables of calculated and observed XRD patterns are deposited in the Supporting Information. The final cell parameters were determined by least squares refinements made on the powder X-ray data, see Table 1.

Infrared Spectroscopy. Infrared (IR) spectra, in the far-IR region (600−50 cm^{-1}), were recorded on a computer-controlled Nicolet 750 Magna-IR Series II spectrophotometer equipped with a TGS/PE detector and silicon beam splitter in 4 cm^{-1} resolution. The samples were ground with dry CsI into a fine powder and pressed into translucent pellets.

Raman Spectroscopy. Raman spectra (600−100 cm^{-1}) were recorded on a BIO-RAD FT Raman spectrometer equipped with a Spectra-Physics Topaz T10−106c 1.064 nm YAG laser and a Ge detector. Crystals of **I**−**III** were loaded without modification into glass capillary tubes. Crystals of **IV** were ground with CsI into a fine powder and loaded into a glass capillary tube.

Single-Crystal Optical Transmission. Room-temperature single-crystal optical transmission spectra were obtained on a Hitachi U-6000 Microscopic FT Spectrophotometer mounted on an Olympus BH2−UMA metallurgical microscope over a wavelenth range of 380 to 900 nm. Crystals lying on a glass slide were positioned over the light source and the transmitted light was detected from above.

Solid-State Ultraviolet (UV)−Visible(Vis)−Near−IR Spectroscopy. Optical diffuse reflectance measurements were performed at room temperature using a Shimadzu UV-3101PC double beam, double monochromator spectrophotometer. The reflectance versus wavelength data generated can be used to estimate the band gap of a material by converting reflectance to absorption data as described earlier.[17]

Differential Thermal Analysis (DTA). DTA experiments were performed on a computer-controlled Shimadzu DTA-50 thermal analyzer. A quartz ampule of equal mass, filled with Al_2O_3, was sealed and placed on the reference side of the detector. The sample was heated to the desired temperature at 10 °C/min, then held there for 10 min, and finally cooled to 50 °C at the same rate. The stability and reproducibility of the samples were monitored by running multiple cycles. Residues of the DTA experiment were examined by X-ray powder diffraction. To evaluate congruent melting, the X-ray powder diffraction patterns before and after the DTA experiments were compared.

Semiquantitative Microprobe Analyses. The analyses were performed using a JEOL JSM-6400V scanning electron microscope (SEM) equipped with a TN 5500 energy-dispersive spectroscopy (EDS) detector. This technique was used to confirm the presence of all elements in the compounds.

Electronic Structure Calculations. The band structure was calculated using density functional theory with the local density approximation. The one-electron Shrödinger equation was solved self-consistently using the tight binding (TB) linear muffin-tin orbital (LMTO) method in the atomic spheres approximation (ASA), including the combined correction.[18] This method splits the crystal space into overlapping atomic spheres (Wigner−Seitz spheres), whose radii are chosen to completely fill the crystal volume. In the present calculation, 29 additional empty spheres (E) had to be included to model the interstitial space. We allowed an overlap of 15% for the atoms centered spheres, 20% for the interstitial spheres with atomic ones, and 25% between empty spheres. A summary of the sphere radii used in our calculation is given in ref 19. All reciprocal space integrations were performed with the tetrahedron method [20] using 128 k-points within the irreducible Brillouin zone. The basis sets consisted of 4s, 4p, and 3d orbitals for Cu, 3s and 3p orbitals for P and S, and 4s orbitals for K. The 3d orbitals for P and S, the 4p and 3d orbitals for K, and E p−d states were downfolded using the Lowdin's technique.[20]

Single-Crystal X-ray Crystallography. Intensity data for **I** were collected using a STOE Image Plate X-ray diffractometer for room-temperature data collection. The data were collected as a series of diffraction patterns recorded by rotating a randomly oriented crystal in the X-ray beam. Images were recorded over the range $\phi = 0.0°$ to 200.2° with a 0.7° increment angle and a 4 min irradiation per image. Cell parameters were determined from a least-squares analysis of the setting angles of 5000 reflections in the $3.8° = 2\theta = 56.3°$ domain and led to the parameters $a = 6.8307(3)$ Å, $b = 23.565(1)$ Å, $c = 9.5398(5)$ Å, $\beta = 100.213(5)°$. The reflection intensities were recorded in the $-18 = h = 18$, $-8 = k = 8$, and $-11 = l = 11$ space. After the Lorentz polarization correction of the 10692 raw data, a set of 4032 reflections with $I = 3\sigma(I)$ was used. A data analysis indicated a 2/m Laue symmetry with limiting conditions consistent with the $P2_1/n$ space group. The structure was then solved from direct methods using the SHELXTL program[21a] and refined using the JANA'96[21b] software package. Conventional atomic and anomalous scattering factors were taken from the usual sources. The atomic parameters and the scale factor were refined in a full matrix mode minimizing the function $wR = [\Sigma w(|F_o| - |F_c|)^2/\Sigma wF_c^2]^{1/2}$. A weighting scheme based on $\sigma(F_o)$ corrected with an instability coefficient was used. No anharmonic refinement was needed to account for the behavior of the Cu atom.[22]

Intensity data for **III**, and **IV** were collected using a Rigaku AFC6S four-circle automated diffractometer equipped with a graphite crystal monochromator. Unique data for **III**−**IV** were

(16) (a) Yvon, K.; Jeitschko, W.; Parthé, E. *J. Appl. Crystallogr.* **1977**, *10*, 73−74; (b) *CERIUS*^{2}, Version 1.6, Molecular Simulations Inc., Cambridge, England, 1994.

(17) McCarthy, T. J.; Ngeyi, S.-P.; Liao J.-H.; DeGroot, D.; Hogan, T.; Kannewurf, C. R.; Kanatzidis, M. G. *Chem. Mater.* **1993**, *5*, 331−340.

(18) (a) Andersen, O. K. *Phys. Rev. B*, **1975**, *12*, 3060; (b) Andersen, O. K. Jepsen, O. *Phys. Rev. Letter*, **1984**, *53*, 2571; (c) Jepsen, O.; Andersen, O. K. *Z. Phys.* **1995**, *97*, 35.

(19) Cu, 1.50 Å; P(1), 1.15 Å; P(2), 1.13 Å; P(3), 1.15 Å; K(1), 2.43 Å; K(2), 2.54 Å; S(1), 1.17 Å; S(2), 1.15 Å; S(3), 1.15 Å, S(4), 1.15 Å; S(5), 1.14 Å; S(6), 1.30 Å; S(7), 1.31 Å; S(8), 1.30 Å; S(9), 1.13 Å.

(20) (a) Jepsen, O.; Andersen, O. K. *Solid State Comm.* **1971**, *9*, 1763; (b) Lambrecht, W. R. L.; Andersen, O. K. *Phys. Rev. B* **1986**, *34*, 2439.

(21) (a) Sheldrick, G. M. "*SHELXTL version 5*"; Siemens Analytical X-ray Instruments: Madison, WI; (b) Petricek, V.; Dusek, M. "*JANA'96* Crystallographic Computing System"; Institute of Physics, Academy of Sciences of the Czech Republic: Praha, Czech Republic.

(22) van der Lee, A.; Evain, M.; Boucher, F.; Brec, R. *Z. für Kristallogr.* **1993**, *203*, 247−264.

Table 2. Fractional Coordinates and Equivalent Isotropic Atomic Displacement Parameters of $K_2CuP_3S_9$

atom	*x*	*y*	*z*	U_{eq} (Å ^{2})[a]
Cu	0.5680(2)	0.10816(4)	0.3090(1)	2.82(3)
P(1)	0.0638(3)	0.09784(8)	0.3424(2)	1.95(6)
P(2)	0.8170(3)	0.22278(8)	0.2188(2)	2.22(6)
P(3)	0.7605(3)	0.10134(9)	0.0083(2)	2.21(6)
S(1)	0.5812(3)	0.20591(8)	0.3076(2)	2.96(7)
S(2)	0.3344(3)	0.07180(9)	0.4305(2)	2.56(6)
S(3)	0.8552(3)	0.07125(8)	0.4477(2)	2.44(6)
S(4)	0.5203(3)	0.07496(9)	0.0784(2)	3.04(7)
S(5)	0.2202(4)	0.92047(9)	0.1886(2)	3.30(7)
S(6)	0.0275(3)	0.06800(8)	0.1301(2)	2.49(6)
S(7)	0.0840(3)	0.18772(8)	0.3359(2)	2.43(6)
S(8)	0.7991(3)	0.19013(8)	0.0110(2)	2.83(7)
S(9)	0.8756(3)	0.30300(8)	0.1970(2)	3.28(7)
K(1)	0.1718(4)	0.80449(9)	0.3710(2)	4.59(8)
K(2)	0.2324(4)	0.54614(9)	0.7398(2)	4.86(8)

[a] U(*eq*) is defined as one-third pf the trace of the orthogonalized U_{ij} tensor.

Table 3. Atomic Coordinates (× 10^4) and Equivalent Isotropic Displacement Parameters (Å^2 × 10^3) for $Cs_2Cu_2P_2S_6$

atom	*x*	*y*	*z*	*U*(eq)
Cu(1)	5170(2)	8992(1)	5418(2)	29(1)
Cu(2)	10514(2)	9532(1)	9032(2)	27(1)
P(1)	7820(4)	10377(2)	6670(3)	16(1)
P(2)	12858(4)	1.0412(2)	1.1653(3)	15(1)
S(2)	9921(4)	10755(2)	7360(3)	21(1)
S(3)	12797(4)	9310(3)	10226(3)	21(1)
S(4)	8608(4)	8424(3)	0.8917(3)	2.1(1)
S(5)	7466(4)	9300(3)	5200(3)	25(1)
S(6)	5112(4)	9048(3)	7616(3)	22(1)
S(7)	6604(4)	11692(2)	6203(3)	22(1)
Cs(1)	1118(1)	6828(1)	1190(1)	28(1)
Cs(2)	6380(1)	6518(1)	6720(1)	29(1)

collected out to 50° in 2Θ. Crystal stability was monitored with three standard reflections whose intensities were checked every 150 reflections. No crystal decay was detected for either **III** or **IV**. The space groups were determined from systematic absences and intensity statistics. An empirical absorption correction based on ψ scans was applied to both data sets. An empirical DIFABS correction[23] was applied after full isotropic refinement, following which full anisotropic refinement was performed. The structures of **III**−**IV** were solved by direct methods using SHELXS-86 software,[24a] and refined with full matrix least squares techniques using the TEXSAN software package.[24b]

The complete data collection parameters and details of the structure solution and refinement for **I**, **III**, and **IV** are given in Table 1. The coordinates of all atoms, average temperature factors, and their estimated standard deviations are given in Tables 2 to 4.

3. Results and Discussion

3.1 Description of Structures. *$A_2CuP_3S_9$ (A = K, Rb).* Because these two compounds are isostructural, the discussion here will refer mainly to the K^+ salt. The structure of $K_2CuP_3S_9$ consists of infinite straight chains of $[CuP_3S_9]_n^{2n-}$ running along the [100] direction, see Figure 1. The shortest measured interchain S−S distance is 3.516(3) Å, suggesting that the two potassium cations ensure adequate screening of the anions.

(23) Walker, N.; Stuart. D. *Acta Crystallogr.* **1983**, *A39*, 158−166.
(24) (a) Sheldrick, G. M. In *Crystallographic Computing 3*; Sheldrick, G. M., Kruger, C.; Goddard R., Eds.; Oxford University: Oxford, England, 1985; p 175; (b) *TEXSAN: Single-Crystal Structure Analysis Software*, Version 1.7; Molecular Structure Corp.: 3200 Research Forest Drive, The Woodlands, TX, 1995.

Table 4. Atomic Coordinates (× 10^4) and Equivalent Isotropic Displacement Parameters (Å^2 × 10^3) for $K_3CuP_2S_7$

atom	*x*	*y*	*z*	$U_{(eq)}$
Cu(1)	674(1)	223(3)	8046(1)	31(1)
P(1)	1134(2)	5007(5)	8380(2)	20(1)
P(2)	1676(2)	−2404(5)	6459(2)	21(1)
S(1)	17(2)	3024(5)	8600(2)	25(1)
S(2)	838(2)	5184(5)	6938(2)	22(1)
S(3)	921(3)	0.0196(5)	0.6625(2)	28(1)
S(4)	861(3)	−2377(5)	8974(2)	29(1)
S(5)	3138(2)	−0.2368(5)	7070(2)	28(1)
S(6)	2534(2)	3927(6)	8812(2)	32(1)
S(7)	1480(3)	−3104(6)	5144(2)	29(1)
K(1)	3187(2)	2611(5)	6961(2)	36(1)
K(2)	3437(3)	8518(6)	9289(2)	45(1)
K(3)	963(2)	2214(5)	4726(2)	35(1)

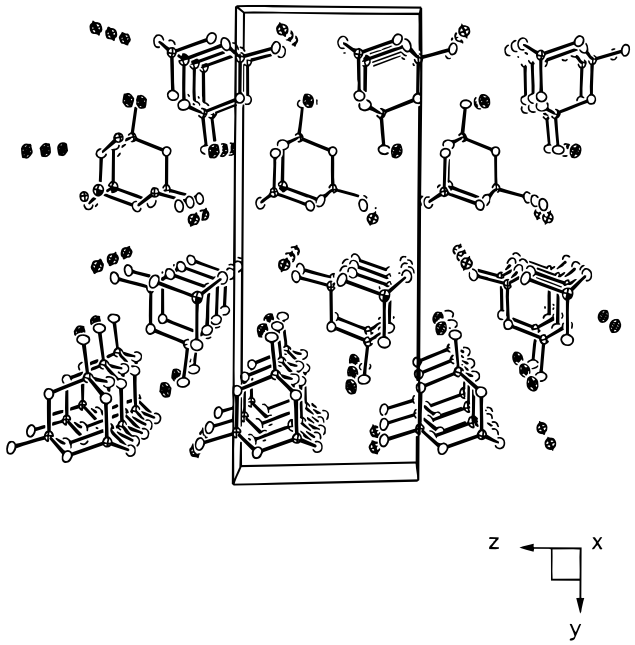

Figure 1. ORTEP representation of $K_2CuP_3S_9$ down the *a*-axis (50% probability ellipsoids). Small shaded ellipsoids, Cu; small crossed ellipsoids, P atoms; open ellipsoids, S; and large crossed ellipsoids, K.

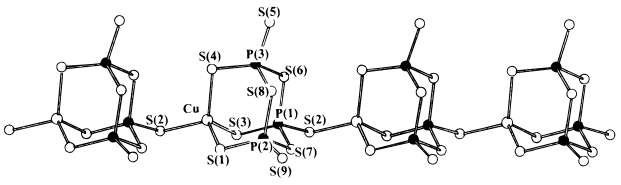

Figure 2. Perspective view of a $[CuP_3S_9]^{2-}$ chain with the labeling scheme.

The chains are built up from $[CuS_4]$ tetrahedra bonded to the newly observed cyclic $[P_3S_9]^{3-}$ units. The only other remotely related species we could find is the binary sulfide P_4S_9, which has an adamantane structure where one of the phosphorus vertexes has been reduced to a P^{3+} center. The cyclic $[P_3S_9]^{3-}$ unit is the result of three corner-sharing $[PS_4]^{3-}$ tetrahedra. As shown in Figure 2, the basal plane of a $[CuS_4]$ tetrahedron defined by S(1), S(3), S(4) is common to one $[P_3S_9]^{3-}$ unit whereas the fourth apical sulfide [S(2)] of the copper tetrahedron is shared with a second neighboring $[P_3S_9]^{3-}$ unit. The structure can also be described in terms of a basic building block, the adamantane-like $[CuP_3S_9]^{2-}$ cluster. These derivative adamantane clusters link to

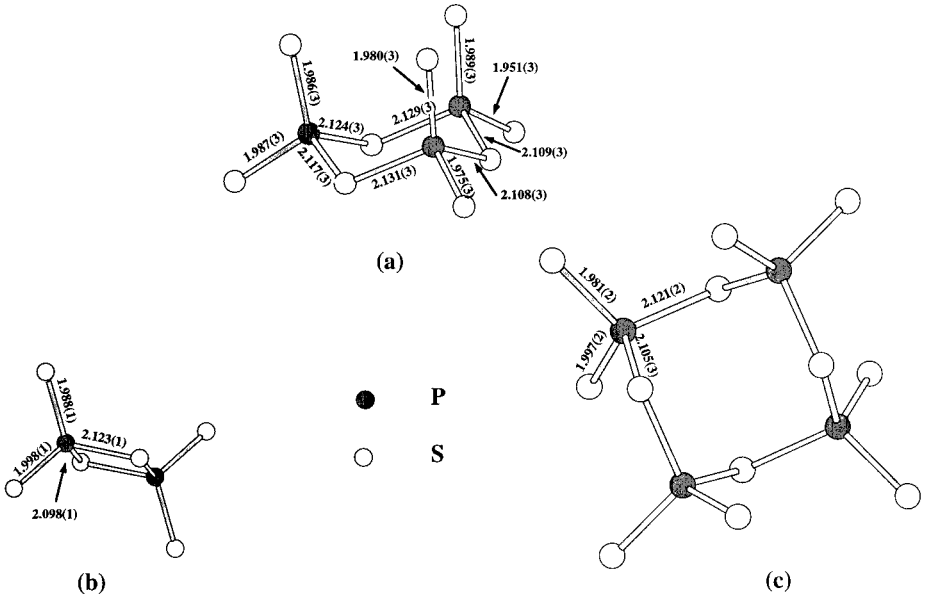

Figure 3. Perspective views of (a) the tri-tetrahedral $[P_3S_9]^{3-}$ ring observed in $K_2CuP_3S_9$ (b), the bitetrahedral $[P_2S_6]^{2-}$ ring, and (c) the quadri-tetrahedral $[P_4S_{12}]^{4-}$ observed, respectively, in 2D and 3D NbP_2S_8.

form a one-dimensional structure via the coordinative interaction of a terminal sulfide from one $[CuP_3S_9]^{2-}$ cluster to a copper atom of a neighboring $[CuP_3S_9]^{2-}$ cluster, filling the apical position of the $[CuS_4]$ tetrahedron. The $[CuP_3S_9]_n^{2-}$ chains are highly acentric in nature (see Figure 2), but pack in a centrosymmetric fashion, preventing any macroscopic polarization to develop in the material. The Cu−S distances range from 2.299(2) to 2.332(2) Å. The average Cu−S distance of 2.310(3) Å in **I** compares well with previously studied compounds with tetrahedral $[CuS_4]$ groups.[25] The S−Cu−S angles range from 99.49(8) to 114.00(9)°. A perspective view of the $[P_3S_3]$ ring that highlights the chair configuration of the six-membered ring of the trimetathiophoshate is shown in Figure 3. The $[P_3S_9]^{3-}$ unit represents a new member of the $[P_nS_{3n}]^{n-}$ anionic series of ring structures including the $[P_2S_6]^{2-}$ anion[26] and $[P_4S_{12}]^{4-}$ anion[27] encountered in the two-(2D) and three-dimensional (3D) forms of NbP_2S_8 (see Figures 3b and 3c).

In the $[P_3S_9]^{3-}$ unit, the P−S distances range from 1.951(3) to 2.131(3) Å, with average P−S distances of 2.054(3), 2.045(3), and 2.049(3) Å for P(1), P(2), and P(3), respectively. The distances compare well with the sum of the ionic radii (rS^{2-} = 1.84 Å, rP^{5+} = 0.17 Å) and those previously reported.[3] The S−P−S angles reveal only a slight deviation from tetrahedral coordination and range from 103.4(1) to 116.1(1)°. Selected bond distances and angles for $K_2CuP_3S_9$ are given in Table 5. The phosphorus atoms of the $[P_3S_3]$ chair-shaped ring define an almost equilateral triangle with a mean P−P−P angle of 60.00(5)° and a mean P−P distance of 3.483(3) Å.

Table 5. Selected Bond Distances (Å) and Angles (°) in $K_2CuP_3S_9$

bond	distance (Å)	angle	degree
Cu−S(1)	2.305(2)	S(1)−Cu−S(2)	114.00(9)
Cu−S(2)	2.299(2)	S(1)−Cu−S(3)	110.25(8)
Cu−S(3)	2.332(2)	S(1)−Cu−S(4)	109.43(8)
Cu−S(4)	2.303(2)	S(2)−Cu−S(3)	99.49(8)
		S(2)−Cu−S(4)	111.23(8)
		S(3)−Cu−S(4)	112.18(8)
P(1)−S(2)	1.987(3)	S(2)−P(1)−S(3)	112.7(1)
P(1)−S(3)	1.986(3)	S(2)−P(1)−S(6)	104.1(1)
P(1)−S(6)	2.117(3)	S(2)−P(1)−S(7)	105.0(1)
P(1)−S(7)	2.124(3)	S(3)−P(1)−S(6)	114.0(1)
		S(3)−P(1)−S(7)	112.7(1)
		S(6)−P(1)−S(7)	107.5(1)
P(2)−S(1)	1.989(3)	S(1)−P(2)−S(7)	112.5(1)
P(2)−S(7)	2.129(3)	S(1)−P(2)−S(8)	114.3(1)
P(2)−S(8)	2.109(3)	S(1)−P(2)−S(9)	115.8(1)
P(2)−S(9)	1.951(3)	S(7)−P(2)−S(8)	104.7(1)
		S(7)−P(2)−S(9)	105.0(1)
		S(8)−P(2)−S(9)	103.4(1)
P(3)−S(4)	1.980(3)	S(4)−P(3)−S(5)	116.1(1)
P(3)−S(5)	1.975(3)	S(4)−P(3)−S(6)	112.4(1)
P(3)−S(6)	2.131(3)	S(4)−P(3)−S(8)	114.6(1)
P(3)−S(8)	2.108(3)	S(5)−P(3)−S(6)	103.1(1)
		S(5)−P(3)−S(8)	103.9(1)
		S(6)−P(3)−S(8)	105.4(1)

It is worth noting that there are two types of P−S distances in the $[P_3S_9]^{3-}$ unit. The average P−S distances in the $[P_3S_3]$ ring are slightly longer than the average terminal P−S distances, (2.121(1) versus 1.978(4) Å) for the bridging and terminal distances, respectively (see Figure 3). A similar trend is observed in the bi-tetrahedral $[P_2S_6]^{2-}$ [2.111(1) versus 1.993(1) Å],[26] and quadri-tetrahedral $[P_4S_{12}]^{4-}$units [2.113(3) versus 1.989(2) Å],[27,28] respectively. In oxides, this segregation is more pronounced. Hence, from the structures of anhydrous sodium trimetalphosphate $Na_3P_3O_9$, and the monohydrate $Na_3P_3O_9,H_2O$,[29] the average P−O $[P_3O_3]$ ring distance is 1.615 Å and the average terminal P−O distance is 1.484 Å.

The $[CuP_3S_9]^{2-}$ chains are separated by A^+ ions that are located in two different sites. In $K_2CuP_3S_9$, the K(1)

(25) (a) Liao, J.-H.; Kanatzidis, M. G. *Chem. Mater.* **1993**, *5*, 1561; (b) Keane, P. M.; Lu, Y.-J.; Ibers, J. A. *Acc. Chem. Res.* **1991**, *24*, 223; (c) Lu, Y.-J.; Ibers, J. A. *J. Solid State Chem.* **1992**, *98*, 312.

(26) (a) Grenouilleau, P.; Brec, R.; Evain, M.; Rouxel, J. *Rev. Chim. Miner.* **1983**, *20*, 628; (b) Bouchetière, M.; Toffoli, P.; Khodadad, P.; Rodier, N. *Acta Crystallogr.* **1978**, *B34*, 384.

(27) Evain, M.; Brec, R.; Ouvrard, G.; Rouxel, J. *Mater. Res. Bull.* **1984**, *19*, 41.

(28) Queignec, M.; Evain, M.; Brec, R.; Sourisseau, C. *J. Solid State Chem.* **1986**, *63*, 89.

(29) Ondik, H. *Acta Crystallogr.* **1965**, *18*, 226.

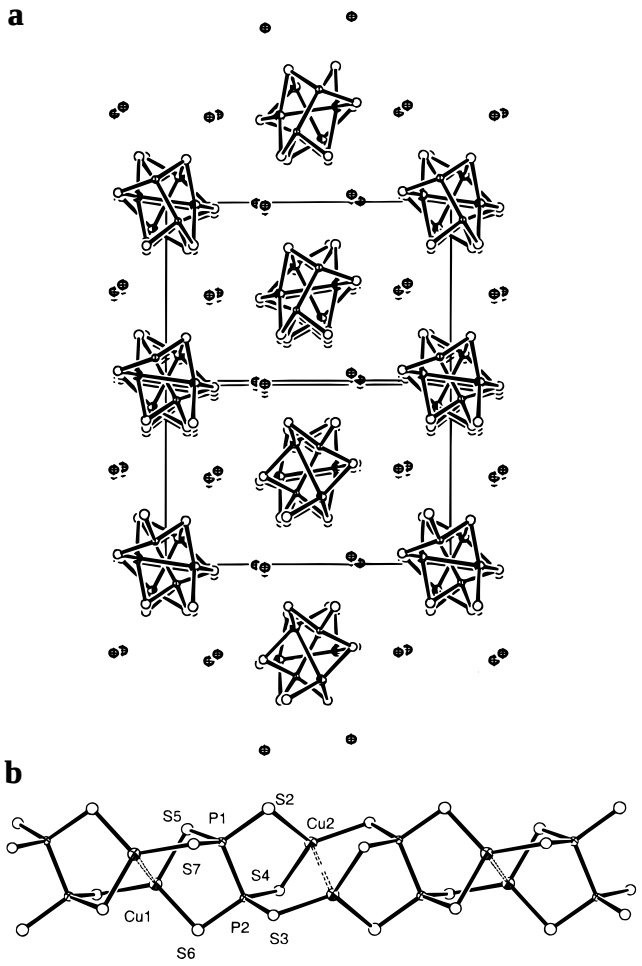

Figure 4. (a) Packing diagram of $Cs_2Cu_2P_2S_6$ as viewed along the [101] direction. (B) View of a single $[Cu_2P_2S_6]^{2n-}$ chain with labeling.

atom is in 8-fold coordination with sulfur atoms [range of K(1)−S distances, 3.200(3) to 3.688(3) Å; average 4.418(3) Å] and the K(2) atom is surrounded by nine sulfur atoms [range of K(2)−S distances, 3.286(3) to 3.767(3) Å; average 3.515(3) Å].

$Cs_2Cu_2P_2S_6$ (III). $Cs_2Cu_2P_2S_6$ is isostructural to the previously reported selenide analogue.[5a] In this compound, alternating ethane-like $[P_2S_6]^{4-}$ units linked to Cu_2^{2+} dimers form infinite chains which run along the [101] direction (Figure 4a). These chains pack side by side in a pseudohexagonal motif (see Figure 4b). This one-dimensional structure is closely related to that of $KMnP_2S_6$.[30a] The average Cu−Cu distance in $Cs_2Cu_2P_2S_6$ is 2.720(5) Å, slightly shorter than that reported for $Cs_2Cu_2P_2Se_6$ at 2.746(5) Å, and most likely reflects the presence of $d^{10}-d^{10}$ interactions. The P−P distance of 2.242(7) Å in **III** is slightly longer than the average P−P distance of 2.21(1) Å reported for $KMnP_2S_6$,[30a] $KFeP_2S_6$,[30b] and $Na_{0.16}Bi_{1.28}P_2S_6$.[31] The P−P distance of 2.242(7) Å observed for **III** is shorter than the P−P distance of 2.260(6) Å observed for $Cs_2Cu_2P_2Se_6$. Selected bond distances and angles for $Cs_2Cu_2P_2S_6$ are given in Table 6.

Table 6. Selected Distances (Å) and Angles (deg) for $Cs_2Cu_2P_2S_6$ with Standard Deviations in Parentheses[a]

bond	distance (Å)	angle	degree
P(1)−S(1)	2.025(8)	S(1)−P(1)−S(2)	1113.8(2)
P(1)−S(2)	2.020(7)	S(1)−P(1)−S(3)	110.0(2)
P(1)−S(3)	2.032(7)	S(2)−P(1)−S(3)	113.5(2)
		S(1)−P(1)−P(2)	106.0(2)
P(2)−S(4)	2.032(7)	S(2)−P(1)−P(2)	105.0(2)
P(2)−S(5)	2.023(7)	S(4)−P(1)−P(2)	108.0(2)
P(2)−S(6)	2.014(8)		
P(1)−P(2)	2.245(5)	S(4)−P(2)−S(5)	113.3(2)
		S(4)−P(2)−S(6)	111.5(2)
Cu(1)−S(1)	2.293(4)	S(5)−P(2)−S(6)	112.9(2)
Cu(1)−S(2)	2.307(4)	S(4)−P(2)−P(1)	107.8(2)
Cu(1)−S(3)	2.264(4)	S(5)−P(2)−P(1)	104.7(2)
		S(6)−P(2)−P(1)	106.6(2)
Cu(2)−S(4)	2.314(4)		
Cu(2)−S(5)	2.262(4)		
Cu(2)−S(6)	2.293(4)	Cu(1)−Cu(1′)−S(2)	81.1(1)
		Cu(1)−Cu(1′)−S(6)	105.1(1)
Cu(1)−Cu(1′)	2.716(3)	Cu(1)−Cu(1′)−S(3)	96.8(1)
Cu(2)−Cu(2′)	2.724(3)		
		S(2)−Cu(1)−S(6)	109.6(1)
		S(2)−Cu(1)−S(3)	124.0(1)
		S(6)−Cu(1)−S(3)	124.4(1)
		Cu(2)−Cu(2′)−S(1)	101.4(1)
		Cu(2)−Cu(2′)−S(4)	96.6(1)
		Cu(2)−Cu(2′)−S(6)	83.4(1)
		S(1)−Cu(2)−S(4)	109.2(1)
		S(1)−Cu(2)−S(5)	122.2(1)
		S(4)−Cu(2)−S(5)	127.2(1)

[a] The estimated standard deviations in the mean bond lengths and the mean bond angles are calculated by the equation $\sigma l = \{\Sigma_n(l_n - l)^2/n(n-1)\}^{1/2}$, where l_n is the length (or angle) of the nth bond, l is the mean length (or angle), and n is the number of bonds.

$K_3CuP_2S_7$ (IV). This compound contains infinite straight chains of $[CuP_2S_7]_n^{3n-}$, which are parallel to the crystallographic *a*-axis (Figure 5a) and are well separated by K^+ cations (Figure 5b). The overall $[CuP_2S_7]_n^{3n-}$ chain structure is related to that of $A_2CuP_3S_9$ where the novel $[P_3S_9]^{3-}$ unit is replaced by the $[P_2S_7]^{4-}$ (pyrothiophosphate) unit. The pyrothiophosphate $[P_2S_7]^{4-}$ unit consists of two corner-sharing $[PS_4]^{3-}$ tetrahedra and it has been previously observed in $ABiP_2S_7$ (A = K, Rb),[32] $RbVP_2S_7$,[33] and $AAuP_2S_7$ (A = K, Rb).[3] The Cu^+ cation is in a trigonal planar coordination with Cu−S bond distances ranging from 2.226(4) to 2.278(4) Å and S−Cu−S angles in the range from 115.3(1) to 125.7(2)°.

The coordination environment of the coinage metal site in **III** and $AAuP_2S_7$ (A = K, Rb) is worth discussing here. The square planar coordination of the Au^{3+} ions is formed by bonding to two of the three terminal sulfides from each PS_4 tetrahedron. The binding scheme for the coordination of the Cu^+ ions in **IV** is completely different. One $[P_2S_7]^{4-}$ unit chelates in a bidentate fashion to the Cu^+ ion and the third coordination site is filled by a sulfide from a neighboring $[P_2S_7]^{4-}$ unit.

The structure of **IV** is related to that of **I** because the chains are constructed by two of the terminal sulfides of the polythiophosphate units binding to one Cu^+ ion and then bridging the neighboring Cu^+ ion. In **I**, the $[P_3S_9]^{3-}$ unit chelates in a tridentate fashion, forming the basal plane of the coordination sphere. The removal

(30) (a) Menzel, F.; Brockner, W.; Carrillo-Cabrera, W.; von Schnering H. G. *Z. Anorg. Allg. Chem.* **1994**, *620*, 1081; (b) Carrillo-Cabrera, W.; Sabmannshausen, J.; von Schnering H. G.; Menzel, F.; Brockner, W. *Z. Anorg. Allg. Chem.* **1994**, *620*, 489.

(31) McCarthy, T. J.; Kanatzidis, M. G. *J. Alloys Compd.* **1996**, *236*, 1089.

(32) McCarthy, T. J.; Hogan, T.; Kannewurf, C. R.; Kanatzidis, M. G. *Chem. Mater.* **1994**, *6*, 1072−1079.

(33) Durand, E.; Evain, M.; Brec. R. *J. Solid State Chem.* **1992**, *102*, 146.

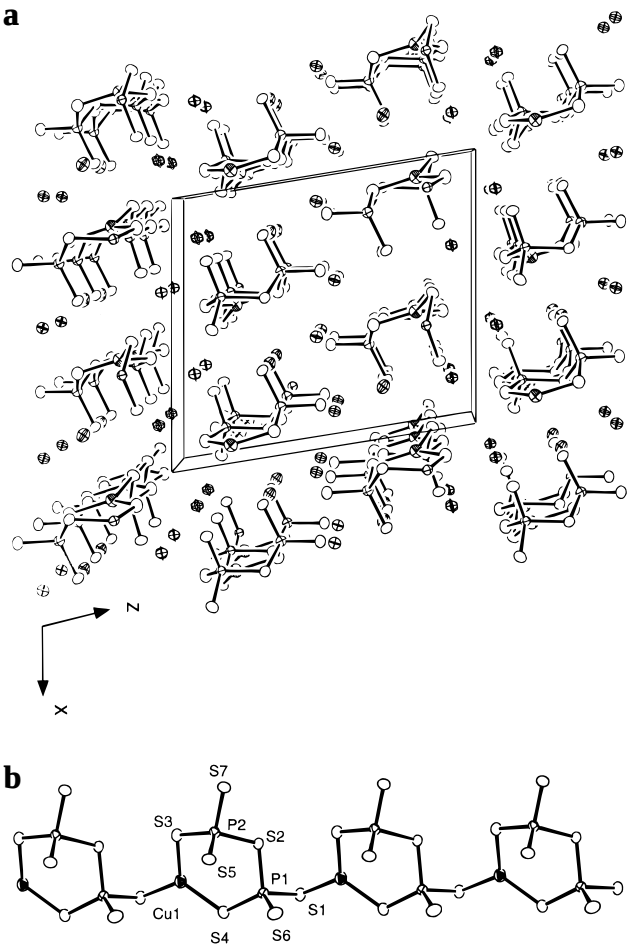

Figure 5. (a) ORTEP representation of a single $[CuP_2S_7]^{2n-}$ chain with labeling. (b) View of $K_3CuP_2S_7$ as viewed down the *b*-axis.

of a second $[PS_2]$ vertex results in the $[P_2S_7]^{4-}$ unit that chelates in bidentate fashion to the Cu^+ ion, forming six-membered rings. This coordination twists the $[P_2S_7]^{4-}$ unit, preventing the Cu^+ ion from adopting a tetrahedral coordination environment. Each PS_4 tetrahedron is slightly distorted with P−S distances ranging from 1.987(4) to 2.167(4) Å, and S−P−S angles ranging from 99.2(2) to 115.5(2)°, respectively. Selected bond distances and angles are given in Table 7.

The potassium cations are located in three different sites. In $K_3CuP_2S_7$, K(1) is coordinated by seven sulfur atoms [range of K(1)−S distances, 3.178(5)−3.527(5) Å; average, 3.32(4) Å]. K(2) and K(3) are also seven-coordinated [3.325(5)−3.531(5) Å, average, 3.38(1) Å; and 3.137(4)−3.642(5) Å; average, 3.31(4) Å, respectively].

3.2 Synthesis and Comparison between the Thiophosphate and Selenophosphate Fluxes. Throughout our exploration we have observed a significant difference between the thiophosphate and selenophosphate systems. The thiophosphate flux appears to favor the P^{5+} species, whereas the selenophosphate flux displays a tendency to favor the reduced P^{4+} species. The stability of the reduced P^{4+} species is consistent with the lower oxidizing power of the Se_x^{2-} ligands compared with S_x^{2-} ligands.

The Lewis basicity of chalcophosphate flux controls the nature of the $[P_xQ_y]^{n-}$ units observed. In the selenophosphate system, the basicity is controlled by changing the A_2Se concentration, and in the thiophosphate system varying the P_2S_5 concentration changes the Lewis basicity. The tetrahedral $[PQ_4]^{3-}$ (Q = S, Se) unit is observed in both systems under highly basic conditions (high A_2Q or low P_2Q_5). Whereas the $[P_2Se_6]^{4-}$ unit is repeatedly observed under less Lewis basic conditions (low A_2Q), occasionally other reduced phosphorus species have been observed.[5d] Further increasing the Lewis acidity, as observed in the synthesis of $K_2Cu_2P_4Se_{10}$,[5f] condenses two $[P_2Se_6]^{4-}$ units together via bridging selenides, forming another new unit the $[P_4Se_{10}]^{4-}$ that has a cyclohexane-like ring.

In contrast, in the thiophosphate system, decreasing the Lewis basicity of the flux (i.e., higher P_2S_5 concentration) favors the formation of higher order $[P_xS_y]^{n-}$ units with phosphorus centers mainly in the +5 oxidation state. To further explore these phosphorus-rich conditions, the elemental sulfur was removed from the reaction conditions. A molten thiophosphate flux is still formed by the combination of A_2S and P_2S_5, but the oxidative properties are different because of the absence of S−S bonds. Here a portion of the thiophosphate flux becomes sacrificial, oxidizing the coinage metal. The formation of the P^{4+} center in $Cs_2Cu_2P_2S_6$ is rationalized this way. The exact influence of these phosphorus-rich conditions on product outcome is not well understood.

Table 7. Selected Distances (Å) and Angles (deg) for $K_3CuP_2S_7$ with Standard Deviations in Parentheses[a]

bond	distance (Å)	angle	degree
P(1)−S(1)	2.039(5)	S(1)−P(1)−S(2)	100.2(2)
P(1)−S(2)	2.167(4)	S(1)−P(1)−S(4)	108.2
(2)P(1)−S(4)	2.025(5)	S(1)−P(1)−S(7)	111.0(2)
P(1)−S(7)	1.987(5)	S(2)−P(1)−S(4)	112.3(2)
		S(2)−P(1)−S(7)	111.6(1)
P(2)−S(3)	2.043(5)	S(4)−P(1)−S(7)	112.7(2)
P(2)−S(2)	2.138(5)	S−P(1)−S (mean)	109(1)
P(2)−S(8)	2.017(5)		
P(2)−S(5)	1.994(5)	S(2)−P(2)−S(3)	108.5(2)
		S(2)−P(2)−S(5)	111.1(2)
Cu(1)−S(1)	2.278(4)	S(2)−P(2)−S(8)	99.2(2)
Cu(1)−S(3)	2.226(4)	S(3)−P(2)−S(5)	112.5(2)
Cu(1)−S(4)	2.226(4)	S(3)−P(2)−S(8)	109.0(2)
		S(5)−P(2)−S(8)	115.5(2)
		S−P(2)−S (mean)	109(1)
		P(1)−S(2)−P(2)	111.1(2)
		S(1)−Cu−S(3)	118.7(2)
		S(1)−Cu−S(4)	115.3(1)
		S(3)−Cu−(4)	125.7(2)

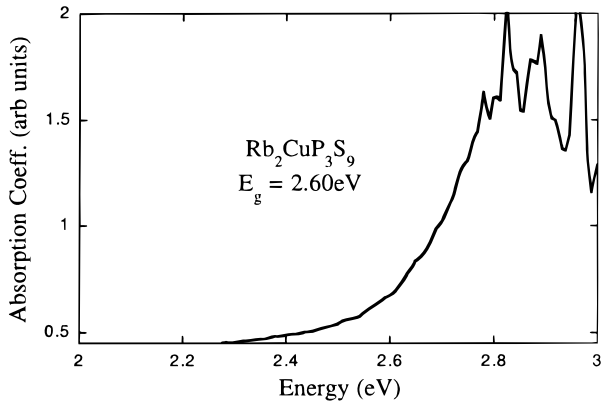

Figure 6. Single-crystal optical absorption spectrum of **II**. The sharp features at high absorbance are noise and due to the very low transmission of light at those energies.

Table 8. IR and Raman Spectroscopic Data for $K_2CuP_3S_9$, $K_3CuP_2S_7$, and $Cs_2Cu_2P_2S_6$

$K_2CuP_3S_9$ **(I)**		$Cs_2Cu_2P_2S_6$ **(III)**		$K_3CuP_2S_7$ **(IV)**	
IR	Raman	IR	Raman	IR	Raman
665(s)	660(w)	574(m)	555(m)	578(m)	
647(sh)	582(m)	441(m)		565(m)	
400(m)	391(s)			463(s)	470(m)
368(m)			367(s)	410(w)	389(s)
350(m)				355(w)	
327(w)	321(m)				
303(m)		314(m)	305(m)		
289(w)	289(w)	287(w)		290(w)	
278(m)			272(w)		
268(w)				263(w)	
253(w)	255(w)				
246(m)		248(w)	250(w)	244(w,b)	
227(s)	224(m)		225(w)	221(w)	217(m)
208(w)			179(w)		
202(m)			147(w)		
196(w)					
169(w)	174(m)				

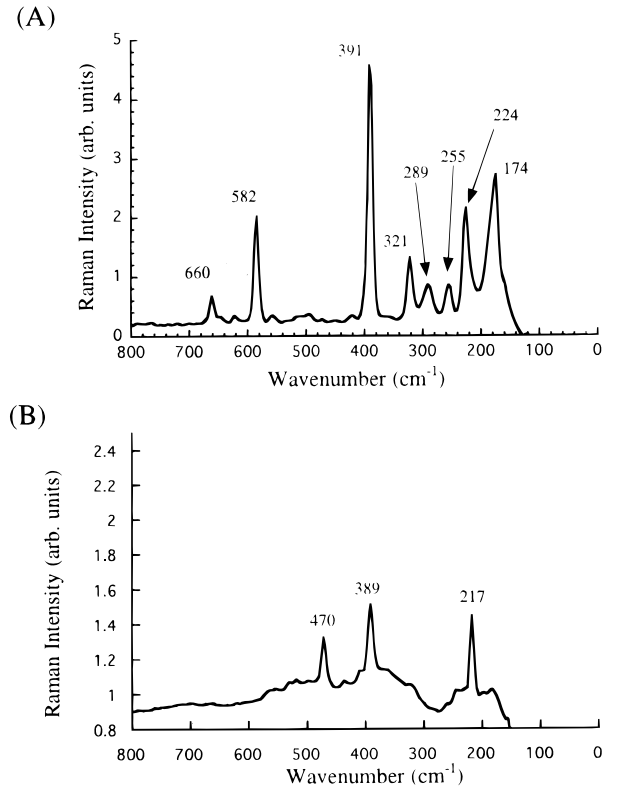

Figure 7. Raman spectra of (A) $K_2CuP_3S_9$ (**I**) and (B) $K_3CuP_2S_7$ (**II**).

Physicochemical Properties. The optical absorption properties of **I**, **II** and **IV** were measured on single crystals. The optical spectrum of **III** was obtained in the diffuse reflectance mode using polycrystalline samples of the compound. The spectra show that these materials are wide band-gap semiconductors. The $A_2CuP_3S_9$ (A = K, Rb,) compounds exhibit band-gaps, E_g, of 2.57 eV **(I)**, and 2.60 eV **(II)**, respectively (see Figure 6), and this result is in agreement with the yellow color of both phases. The nature of the observed gap is explored later in conjunction with the electronic band structure calculations. The band-gap of $Cs_2Cu_2P_2S_6$ is 2.43 eV and that of $K_3CuP_2S_7$ is 2.95 eV.

The far-IR and Raman spectra of **I**, **III**, and **IV** are summarized in Table 8. The far-IR spectra of **I**, **II**, and **IV** display several absorptions in the 600−400 cm^{-1} range. The sharp absorption at 400 and 463 cm^{-1} represents the characteristic P−S−P stretching vibrations for **I** and **IV**, respectively. The doubly bridging bonding motif lowers the energy of the S−P−S vibration for **I** and **II**. The remaining absorptions are tentatively assigned to the $-PS_2$ stretching vibrations by analogy to $AAuP_2S_7$ (A = K, Rb).[3] Absorptions below 400 cm^{-1} are assigned to Cu−S stretching vibrations. The far-IR spectrum of $Cs_2Cu_2P_2S_6$ displays an absorption at 441 cm^{-1}, which may be assigned to the P−P stretching vibration by analogy to $Sr_2P_2S_6$,[34] at 448 cm^{-1}.

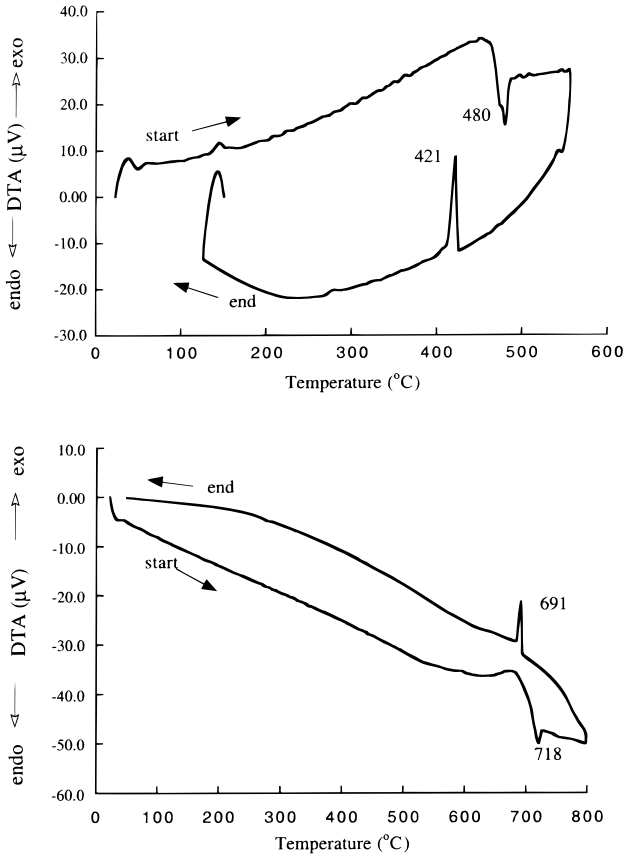

Figure 8. Typical DTA diagrams for $K_2CuP_3S_9$ (**I**, top) and $Cs_2Cu_2P_2S_6$ (**III**, bottom).

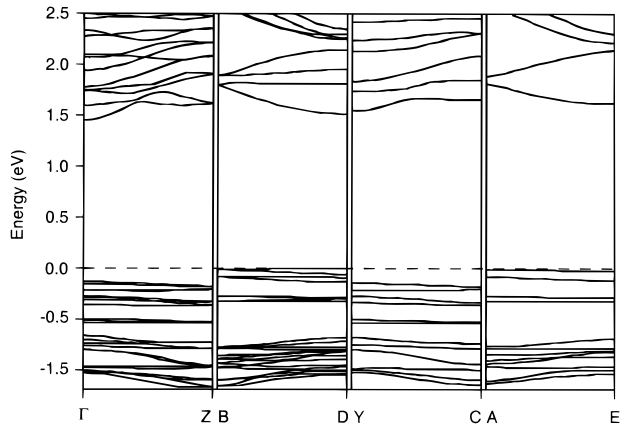

Figure 9. A portion of the electronic band structure in selected directions of reciprocal space. The energy band-gap, which is indirect, is found between the B and Γ points.

(34) Mathey, Y.; Clement, R,; Sourisseau, C.; Lucazeau, G. *Inorg. Chem.* **1980**, *19*, 2773.

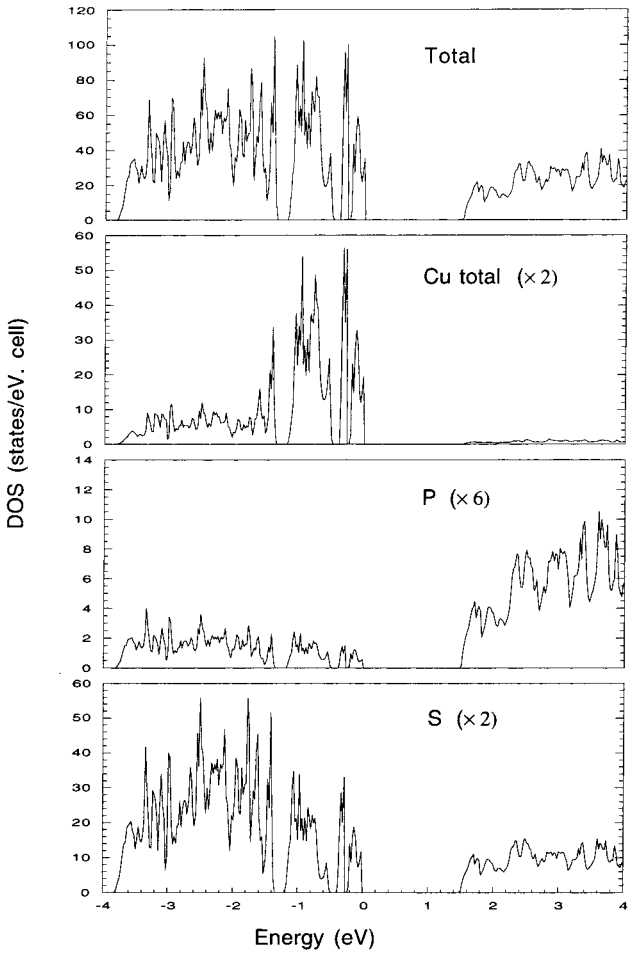

Figure 10. Total density of states and Cu, P, and S projected density of states of $K_2CuP_3S_9$.

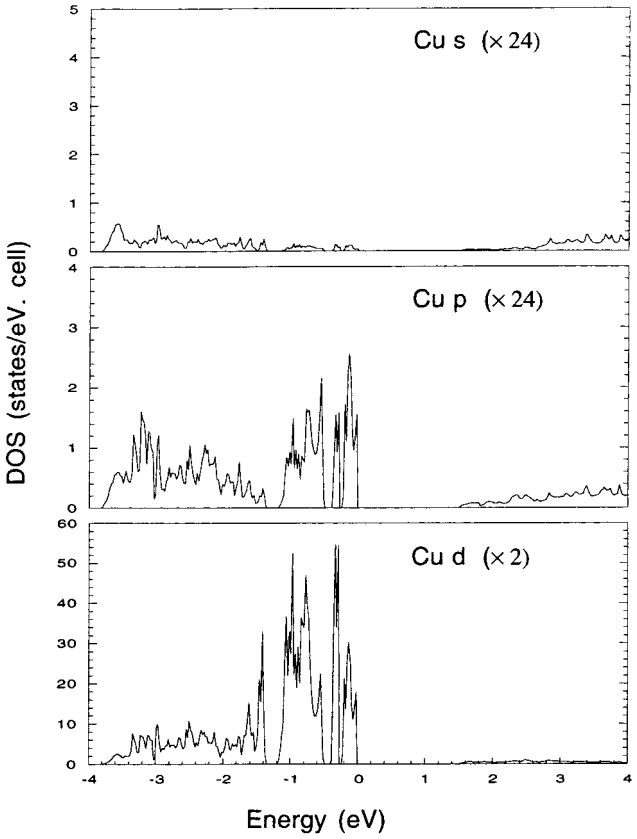

Figure 11. Cu-s, Cu-p, and Cu-d projected density of states of $K_2CuP_3S_9$.

The Raman spectra of **I** and **II** display absorptions in the 250−600 cm^{-1} range that are tentatively assigned to P−S and absorptions below 250 cm^{-1} are assigned to Cu−S stretching vibrations. The sharp absorption at ∼391 cm^{-1} is assigned to the $-PS_3$ stretching vibration by analogy to A_2AuPS_4 and $AAuP_2S_7$ (A = K, Rb).[3] The spectrum of **III** displays several absorptions below 200 cm^{-1} that could be due to Cu−S stretching vibrations. The absorptions above 300 cm^{-1} are tentatively assigned to P−S or P−P vibrations. The Raman spectra of **I** and **IV** are shown in Figure 7.

The DTA data followed by careful X-ray diffraction (XRD) analysis of the residues show that **I** and **II** melt congruently at 472 and 470 °C, respectively. Crystals of **III** melt congruently at 716 °C. The DTA of **IV** shows that it melts incongruently at ∼500 °C to form a mixture of $K_3CuP_2S_7$ and an as of yet unknown phase. Typical thermograms for **I** and **III** are shown in Figure 8.

Band Structure Calculations. Band structure calculations were performed to get insight into the type of band-gap and origin of the yellow color in $K_2CuP_3S_9$. If color originates from an absorption phenomenon, the energy gap between the two energy levels involved in the absorption process is expected to be ∼2.5−2.7 eV, as is indeed observed experimentally (2.6 eV).

The portion of the electronic band structure near the Fermi level is shown in Figure 9. The total and partial density of states of $K_2CuP_3S_9$ are depicted in Figures 10 and 11 in the [−4,4] eV energy range, with the zero energy taken at the last occupied level. From the calculated electronic structure, a semiconductor behavior is predicted with an indirect energy gap of 1.48 eV. Such a value is too small compared with the experimentally determined value to explain the yellow color. Nevertheless, this discrepancy indeed originates from the limitation of the TB-LMTO-ASA method (or more exactly the density functional method), which is known to underestimate the energy gap by ∼50−70%. The indirect nature of the optical band gap is confirmed by the experimental data obtained from single crystals of this compound. Data plots of $(abs)^2$ versus $h\nu$ and $\sqrt{abs}$ versus $h\nu$, shown in Figure 12, can be used to distinguish between a direct and an indirect gap in semiconductors because in solids the energy dependence of the absorption coefficient is quadratic in materials with direct energy gap, whereas in those with indirect gaps, the dependence scales to the square root.[35]

As already mentioned, copper and phosphorus atoms are in a tetrahedral coordination with sulfur. In the corresponding ML_4 tetrahedral isolated molecule, the cation atomic orbitals, engaged in antibonding interactions with chalcogens, are expected to split into d-E and d-T_2 molecular orbitals sets, whereas sp orbitals are located at higher energy and are unoccupied for Cu^+ and P^{5+}. Hence, the uppermost antibonding levels of the valence band (Figure 9), built substantially on copper d orbitals as shown in Figure 10, could be associated with the Cu-d E and Cu-d T_2 blocks. These levels, however, also possess significant sulfur orbital

(35) Hadenfeldt, C.; Hoedel, D. *Z. Anorg. Allg. Chem.* **1996**, *622*, 1495−1500.

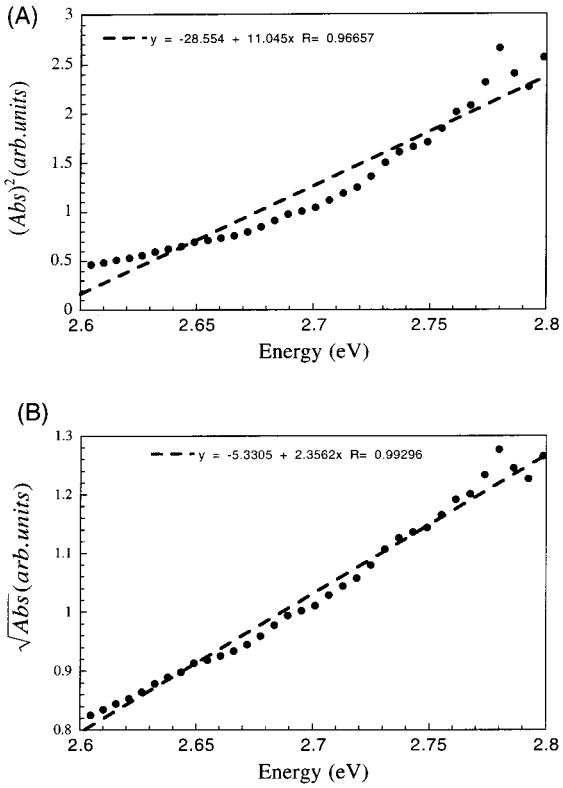

Figure 12. Absorption edge of $K_2CuP_3S_9$ plotted as a function of energy: (A) $(abs)^2$ dependence (direct gap) and (B) $\sqrt{abs}$ dependence (indirect gap).

contributions, in contrast to the bottom of the conduction band (Figures 10), which essentially is constructed from s, p phosphorus orbitals highly hybridized with sulfur orbitals. We note that the charge balance $K^{+}_2Cu^{+}$-$P^{5+}_3S^{2-}_9$ is supported by the band structure calculation if we assign the conduction band completely to sp orbitals of P^{5+}, and the top of the valence band to the copper d levels. The low contribution of the Cu sp orbitals (Figures 10a,b) to the bottom of the conduction band make the occurrence of an intrasite, interband transfer improbable. The yellow color probably originates from a charge transfer from S^{2-} to either Cu^{+} or P^{5+}. Hence, in the absence of any color center impurities, the color process at work in $K_2CuP_3S_9$ would be a light induced heteronuclear intervalence charge transfer.

5. Conclusions

The difference in electronegativity between sulfur and selenium results in spectacular differences in reactivity of the thiophosphate and selenophosphate fluxes. Changing flux conditions (e.g., chalcogenide basicity) results in the formation of various thiophosphate $[P_xS_y]^{n-}$ units. The four compounds reported here support the fact the thiophosphate and selenophosphate systems need to be explored separately. The experimentally observed ability to stabilize higher order thiophosphate units with increased P_2S_5 concentrations endows the system with tremendous flexibility in forming different architectures due to the numerous binding modes of the $[P_xS_y]^{n-}$ units. At this stage we have only a sketchy phenomenological understanding of the complex equilibria between the various P^{5+}-containing species and any $[P_xS_y]^{n-}$ units based on P^{4+} species. We expect nuclear magnetic resonance spectroscopy to be of considerable help in elucidating the equilibrium issues in these systems.

Acknowledgment. Financial support from the National Science Foundation (DMR-9527347) is gratefully acknowledged. M.G.K. is a Camille and Henry Dreyfus Teacher Scholar (1993−1998). This work made use of the SEM facilities of the Center for Electron Optics at Michigan State University.

Supporting Information Available: Tables of fractional atomic coordinates and anisotropic thermal parameters of all atoms, interatomic distances and angles, and calculated and observed X-ray powder patterns for **I**, **III**, and **IV** (25 pages). Ordering information is given on any current masthead page.

CM980175W